

## Exact analytical description of tracer exchange and particle conversion in *single-file* systems

Christian Rödenbeck, Jörg Kärger, and Karsten Hahn

Universität Leipzig, Fakultät für Physik und Geowissenschaften, Linnéstraße 5, D-04103 Leipzig, Germany

(Received 22 November 1996)

The finite single-file system (diffusion in one dimension where the mutual passage of particles is inhibited) with particle exchange at the margins and an attractive nearest-neighbor particle-particle interaction is investigated. As the central quantity, the residence time distribution is introduced and related to experimentally observable quantities concerning tracer exchange and conversion. Exact equations determining these quantities are derived. The numerical solution yields the dependence of these quantities on the system parameters. In addition, the correlations in the single-file system are considered. [S1063-651X(97)02305-2]

PACS number(s): 47.55.Mh, 66.30.-h, 02.50.-r, 05.60.+w

### I. INTRODUCTION

Single-file systems are one-dimensional diffusion systems where the diffusing particles are not able to pass each other. Thus a given order of the particles within the system is strictly maintained. This extreme mutual hindrance of the diffusing particles inhibits counter diffusion and drastically decreases the mobility of the particles: In an infinite single-file system the mean square displacement of a tagged particle increases only proportionally to the square root of the observation time [1] rather than the observation time itself. In lattice gas language, the single-file system corresponds to the one-dimensional exclusion model [2–5]. Note that some authors use the term single file in a less rigorous way, comprising systems with only *restricted* mutual passage as well.

Besides theoretical interest, the investigation of single-file systems has been motivated by a lot of applications, e.g., in the description of superionic or organic conductors [6] or transport through ion channels in biological membranes [7] (for a more detailed summary see the introduction to [2]). Our work is motivated by the diffusional and catalytic processes in the one-dimensional channels of a lot of types of zeolites, e.g., Mordenite, L, AIPO<sub>4</sub>-5, ZSM-12, and many more [8]. Investigations of a great variety of such systems have been reported in the literature [9]. If the diameter of the diffusing guest molecules exceeds the radii of the zeolitic pores, the particles are not able to pass each other any longer and the diffusion obeys single-file behavior, as was evidenced by pulsed field gradient NMR (PFG NMR) measurements with a variety of zeolites and guest species [10]. We are, in particular, interested in two phenomena, namely, tracer exchange and conversion. Experimental findings suggest surprising features in the behavior of such systems, e.g., unusual temperature dependence of chemical reactions [11], which might be attributed to their single-file nature. By investigating a simplified model we aim to elucidate characteristic features allowing an interpretation of experimental results obtained at single-file systems.

In comparison to Fickian diffusion systems, the analysis of single-file systems is considerably complicated by the fact that the motion of a tagged particle is non-Markovian because any displacement is *correlated* to the positions of the other particles and, therefore, to the past dynamical development of the whole system. Because of this difficulty, analyti-

cal results were mainly confined to limiting cases (infinite length, infinite density) or to approximations. The majority of questions could only be answered by numerical simulations. This is what we also did in a previous paper [12] concerning tracer exchange and catalytic reactions in single-file systems. In the present contribution we give both a *model* describing a wider class of systems and an *analytical derivation* for basic quantities. (Throughout this paper, the symbols were chosen consistent to [12].) The model and the formalism are quite general and should be applicable to other questions as well.

In Sec. II the model is presented. It is a lattice gas or Monte Carlo jump model. It is based on simplified interaction potentials motivated by the situation in zeolitic single-file systems [13] but may equally be applied to systems of a different physical nature. The basic quantities are introduced.

In Sec. III we give an exact derivation of sets of equations for these quantities. Numerical evaluation of these sets of equations allows the investigation of their dependence on the parameters of the system. Section IV presents and discusses results concerning the tracer exchange and the conversion. The correlations characteristic of the single-file system are investigated.

### II. MODEL

#### A. Transport dynamics

The single-file system is assumed as a linear chain of  $N$  equidistant sites. These sites correspond to the troughs of a periodic potential describing the interaction of the particles and the channel walls (see Fig. 1). Each pair of adjacent troughs is separated by a potential barrier of height  $E_B$ . If an isolated particle occupies one of the sites, the channel walls can transmit to it a fluctuating energy high enough to overcome this barrier and to jump to a neighboring site. If  $\Gamma dt$  is the probability that the isolated particle performs such an activated jump from a particular site to a particular adjacent one within a time interval of length  $dt$ , the intracrystalline *hop rate of the isolated particle* is given by

$$\Gamma = \hat{\Gamma} e^{-E_B/RT} \quad (1)$$

with the thermal energy  $RT$ . The pre-exponential factor  $\hat{\Gamma}$  is a property of the activation mechanism.

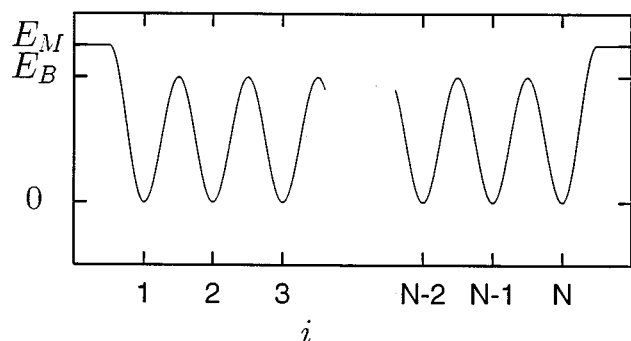


FIG. 1. Energy profile of the channel-particle interaction (schematically).

At the margins, the channel shall be open to a surrounding gas phase. The potential step to be surmounted by an isolated particle at one of the marginal sites 1 or  $N$ , respectively, in order to be desorbed into the gas phase is  $E_M$ . Thus, the *desorption rate of the isolated particle* is

$$\varepsilon = \hat{\varepsilon} e^{-E_M/RT}. \quad (2)$$

Particles from the gas phase do not have to overcome a potential barrier when entering one of the marginal sites of the channel; thus the *adsorption rate of the isolated particle*

$$\alpha = \hat{\alpha} \quad (3)$$

does not depend on temperature and can be related to gas phase properties (e.g., the pressure) and the geometric situation at the channel orifices.

In addition to the channel-particle interaction felt by the isolated particle there is a particle-particle interaction. We introduce a *repulsive* interaction at short particle-particle distances and an *attractive* one at larger distances (see Fig. 2), as may be assumed for small organic molecules. For simplicity the particle-particle potential is assumed to affect adjacent

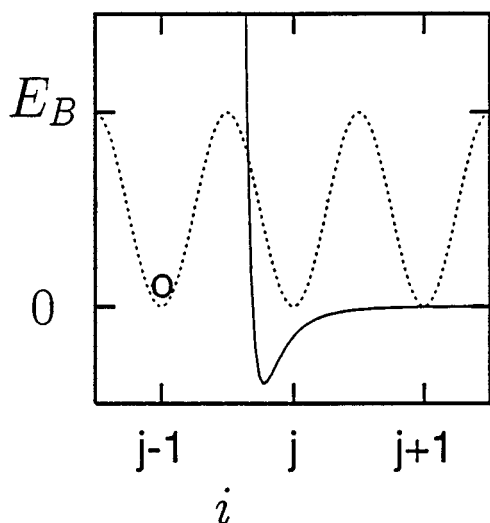


FIG. 2. Additional potential caused by a particle (O) occupying site  $j-1$ .

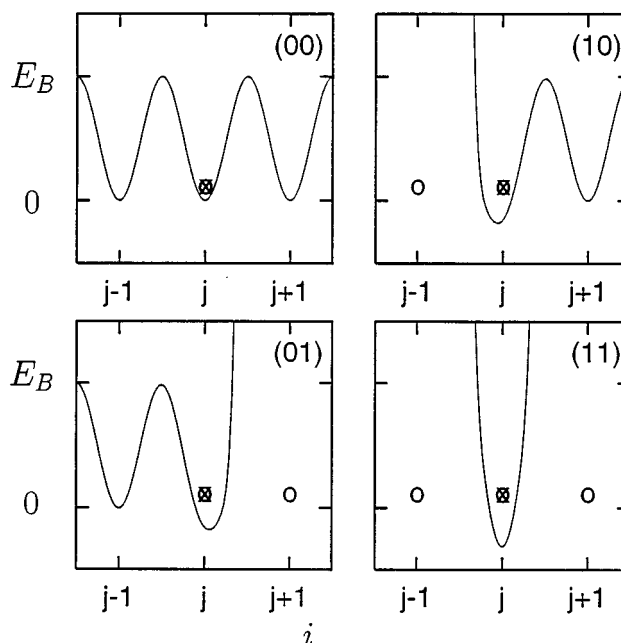


FIG. 3. Total potential felt by the tagged particle ( $\otimes$ ) at the four different configurations of the neighbor particles (O).

sites only. Figure 3 gives the total potential felt by a particle occupying site  $i$  for the four different configurations in the occupation of its neighboring sites  $i-1$  and  $i+1$ . Now consider jumps of this particle to site  $i+1$ . At configuration (00) the *hop rate*  $\Gamma_{(00)}$  will be equal to the hop rate  $\Gamma$  of the isolated particle. At configuration (10) the potential barrier to be surmounted is higher by an interaction energy  $E_I$ , i.e.,  $\Gamma_{(10)} = \hat{\Gamma} e^{-(E_B + E_I)/RT} = \omega \Gamma$ . Here we introduce the *particle-particle interaction parameter*

$$\omega = e^{-E_I/RT}, \quad (4)$$

being the factor by which the hop rate reduces if the hop is directed *away* from an occupied neighboring site. At configurations (01) and (11) a hop to the occupied site  $i+1$  is impossible,  $\Gamma_{(01)} = \Gamma_{(11)} = 0$ . This is the most important consequence of the particle-particle interaction because it inhibits any mutual passage of molecules within the channel and thus causes the *single-file* nature of the system. The same particle-particle influence applies to the adsorption and desorption processes at the margins.

The *parameters*  $\Gamma$ ,  $\varepsilon$ ,  $\alpha$ , and  $\omega$  describe the transport dynamics of the system completely. It is understood that there are no correlations between the hop attempts from different sites or at different times. Physically this implies that any energy transmitted to a particle is given back to the channel walls immediately after the successful, or unsuccessful, hop attempt and dissipates there at once.

## B. Site occupation and residence time

Consider a snapshot of the system at a given time  $t$ . Then two types of information are relevant to our calculations

The first type, the *particle configuration* of the system, shall be described by the set of stochastic variables  $\Sigma_i$  ( $i=1, \dots, N$ ) with

$$\Sigma_i = \begin{cases} 1 \\ 0 \end{cases} \text{ if site } i \text{ is } \begin{cases} \text{occupied} \\ \text{vacant} \end{cases} \quad (5)$$

giving the *occupations* of the individual sites.

The second type of relevant information is the “age structure” of the particles, which shall be represented by stochastic variables  $\tau_i$  defined in the following way:

$$\tau_i = \begin{matrix} \text{(time which the particle occupying} \\ \text{site } i \text{ has already spent within the channel).} \end{matrix} \quad (6)$$

In this definition, the property of the particle (its *residence time*  $\tau_i$ ) is assigned to the site occupied by this particle. If site  $i$  is vacant ( $\Sigma_i=0$ ) the variable  $\tau_i$  is, therefore, an undefined quantity.

Graphically, one might represent the configuration by a linear pattern of blank or inked spots while the “age structure” might be visualized by the respective color of the ink.

Now we define variables determining the *probability distribution* of these stochastic quantities under the assumption that *sorption equilibrium* is attained. The variables  $\Theta_i$  represent the *site occupancies* or the *concentration profile*

$$\Theta_i := P(\Sigma_i = 1), \quad (7)$$

$$1 - \Theta_i = P(\Sigma_i = 0).$$

From the profile one can define the *mean concentration* as

$$\Theta = \frac{1}{N} \sum_{i=1}^N \Theta_i. \quad (8)$$

The variables  $\varphi_i(\tau)$  give the probability densities of the residence times or the *residence time distributions*

$$\varphi_i(\tau) d\tau = P(\tau \leq \tau_i < \tau + d\tau | \Sigma_i = 1) \quad (9)$$

In some cases it is more convenient to replace this conditional probability by a joint probability,

$$\varphi_i^*(\tau) d\tau = P(\Sigma_i = 1, \tau \leq \tau_i < \tau + d\tau) = \Theta_i \varphi_i(\tau) d\tau, \quad (10)$$

distinguished by an asterisk and differing in the *weight factor*  $\Theta_i$ . Throughout this paper, all the quantities derived from these densities wear the asterisk, or not, according to which of these definitions they are based on. Again, one might introduce the *mean residence time distribution* as

$$\varphi(\tau) := \frac{1}{\Theta N} \sum_{i=1}^N \Theta_i \varphi_i(\tau), \quad (11)$$

i.e.,  $\varphi(\tau) d\tau$  gives the ratio between the average number of particles having spent a time between  $\tau$  and  $\tau + d\tau$  within the channel  $\sum_{i=1}^N \Theta_i \varphi_i(\tau) d\tau$  and the average total number of particles  $\Theta N$ .

The sorption equilibrium is always assumed to have been maintained for a time longer than the residence times of all present particles. Then, all these probability distributions are

*stationary*, i.e., they do not vary with time. This fact is most essential to the analytical treatment of the system.

### C. Moments and tracer exchange

We introduce the *m*th moments of the residence time distributions  $\varphi_i(\tau)$ ,

$${}^{(m)}\mu_i = \int_0^\infty \tau^m \varphi_i(\tau) d\tau \quad (12)$$

and their *weighted mean*,

$${}^{(m)}\mu = \frac{1}{\Theta N} \sum_{i=1}^N \Theta_i {}^{(m)}\mu_i. \quad (13)$$

The first moments  ${}^{(1)}\mu_i$  are of special relevance because they give the *average residence times* which can be related to experimentally observable quantities. Tracer exchange experiments [14,15] determine the *intracrystalline mean lifetime* as the integral over the tracer exchange curve  $\gamma(t)$ ,

$$\tau_{\text{intra}} = \int_{t_0}^\infty [1 - \gamma(t)] dt, \quad (14)$$

where  $[1 - \gamma(t)]$  is the relative amount of particles at time  $t$  which have already been within the channel at the initial time  $t_0$ . This is measured by tracking the exchange of two molecular species with equal transport properties, e.g., the deuterated and the normal form of an organic molecule. In the following we shall show that the *dynamically* defined quantity  $\tau_{\text{intra}}$  coincides with the *stationary* mean first moment  ${}^{(1)}\mu$  given in Eq. (13). Using the stochastic variables defined above, the tracer exchange curve can be expressed as

$$1 - \gamma(t) = \frac{\sum_{i=1}^N P(\Sigma_i = 1, \tau_i > t - t_0)}{\sum_{i=1}^N P(\Sigma_i = 1)} = \frac{\sum_{i=1}^N \Theta_i \int_{t-t_0}^\infty \varphi_i(\tau) d\tau}{\sum_{i=1}^N \Theta_i} \quad (15)$$

where we have used Eqs. (7) and (10). Substitution into Eq. (14) yields

$$\tau_{\text{intra}} = \frac{\sum_{i=1}^N \Theta_i \int_{t_0}^\infty dt \int_{t-t_0}^\infty d\tau \varphi_i(\tau)}{\sum_{i=1}^N \Theta_i}. \quad (16)$$

Now we rearrange the integration

$$\int_{t_0}^\infty dt \int_{t-t_0}^\infty d\tau \varphi_i(\tau) = \int_0^\infty d\tau \int_0^\tau dt \varphi_i(\tau) = \int_0^\infty \tau \varphi_i(\tau) d\tau. \quad (17)$$

The second identity is valid only because of the stationarity of the probability density  $\varphi_i(\tau)$ . With Eq. (8) this finally gives the mean first moment according to Eqs. (12) and (13) and we have

$$\tau_{\text{intra}} = {}^{(1)}\mu. \quad (18)$$

#### D. Laplace transform and conversion

Now we consider the irreversible conversion between two species of particles with identical transport properties within the channel. Such systems, e.g., occur in zeolites where the sites are catalytically active. A reactant molecule occupying such an active site will be converted into a product molecule with an *intrinsic reaction rate*

$$k = \hat{k} e^{-E_R/RT}. \quad (19)$$

Due to the exchange processes this product molecule will, after some time, be desorbed into the surrounding gas phase. In return, new reactant molecules will enter the file from the gas phase and diffuse to the active sites so that the reaction can go on. For simplicity we assume that there is such an excess of reactant molecules in the gas phase so that no product molecules are adsorbed again.

Let  $\eta_i^*$  be the probability that site  $i$  is occupied by a *reactant* molecule. Since we assumed that the system has been in sorption equilibrium for a time longer than the residence time of the “oldest” particle, the conversion is in a steady state. This means that the *reactant concentration profile*  $\eta_i^*$  is stationary as well. It can be calculated from the residence time distributions  $\varphi_i^*(\tau)$  by the following argument.  $\varphi_i^*(\tau)d\tau$  is the probability that a given site  $i$  is occupied by a particle and that this particle has spent a time between  $\tau$  and  $\tau+d\tau$  within the channel since its adsorption as a reactant molecule from the gas phase. During this time it had the chance of being converted into a product molecule (this conversion may have happened at an arbitrary time on an arbitrary site). The probability, however, that *no* conversion has taken place is  $e^{-k\tau}$ . The average probability that there is a particle at site  $i$  and that this particle is still a reactant molecule is, therefore, given by

$$\eta_i^* = \int_0^\infty e^{-k\tau} \varphi_i^*(\tau) d\tau. \quad (20)$$

Thus the reactant concentration profile  $\eta_i^*$  happens to be nothing else than the Laplace transform of  $\varphi_i^*(\tau)$ , with  $k$  being the new variable. From the profile one obtains the *mean number of reactant molecules per channel*

$$H^* = \sum_{i=1}^N \eta_i^*. \quad (21)$$

Obviously, this quantity describes the transport influence on the *output rate* of product molecules per channel

$$K = H^* k, \quad (22)$$

and can therefore be related to the *effectiveness factor*  $\eta$  widely used in the theory of heterogeneous catalysis.  $\eta$  is defined as the ratio between the actual output of the transport-reaction system and the output that would be attained if the product molecules were instantaneously replaced by new reactant molecules [15,16]. Thus one has via Eqs. (21) and (22)

$$\eta = \frac{K}{\Theta N k} = \frac{1}{\Theta N} \sum_{i=1}^N \eta_i^*, \quad (23)$$

i.e., the effectiveness factor is given by the weighted mean over the reactant concentration profile.

### III. ANALYTICAL TREATMENT

As shown in the preceding section, the calculation of the concentration profile  $\Theta_i$  and the residence time distributions  $\varphi_i^*(\tau)$  give the key to important quantities of the system. In this section, we derive a set of equations for the probabilities  $\Theta_i$  and a set of differential equations of the densities  $\varphi_i^*(\tau)$ , which can be transferred into sets of linear equations for the moments  ${}^{(m)}\mu_i$  (including the average residence time profile  ${}^{(1)}\mu_i$ ) and the reactant concentration profile  $\eta_i^*$ .

Unfortunately, there are no sets of equations determining these profiles directly. The reason is that the processes at any site are *correlated* to the state (both configuration and “age structure”) of the system as a whole; they are non-Markovian. That is why  $\varphi_i^*(\tau)$  and  $\Theta_i$  are probabilities of the *dependent* set of stochastic variables  $\Sigma_i$  and  $\tau_i$ . Thus we have to look for suitable *joint probabilities* and to calculate the profiles from them by summation. The joint probabilities now refer to a Markov process.

#### A. Concentration profile

At first, we define probabilities of the individual configurations  $(\sigma_1, \sigma_2, \dots, \sigma_N)$  of the system

$$\Theta^{\sigma_1 \sigma_2 \dots \sigma_N} = P(\Sigma_1 = \sigma_1, \Sigma_2 = \sigma_2, \dots, \Sigma_N = \sigma_N). \quad (24)$$

Once these joint probabilities are known the concentration profile can be calculated

$$\Theta_i = \sum_{\sigma_1=0}^1 \dots \sum_{\sigma_{i-1}=0}^1 \sum_{\sigma_{i+1}=0}^1 \dots \sum_{\sigma_N=0}^1 \Theta^{\sigma_1 \dots \sigma_{i-1} 1 \sigma_{i+1} \dots \sigma_N}. \quad (25)$$

The joint probabilities Eq. (24) can be determined by a set of linear equations. In order to understand the course of the calculation, first consider a fictional system with three states (probabilities  $\Theta^{(1)}$ ,  $\Theta^{(2)}$ ,  $\Theta^{(3)}$  and transition rates  $\Gamma_{1 \rightarrow 2}$ ,  $\Gamma_{1 \rightarrow 3}$ , etc.). With, e.g.,  $\Gamma_{1 \rightarrow 2} dt$  being the probability of a transition from state 1 to state 2 occurring during a time interval of length  $dt$ , one has the identity

$$\begin{aligned} \Theta^{(1)}|_{t+dt} &= (1 - \Gamma_{1 \rightarrow 2} dt - \Gamma_{1 \rightarrow 3} dt) \Theta^{(1)}|_t + \Gamma_{2 \rightarrow 1} dt \Theta^{(2)}|_t \\ &\quad + \Gamma_{3 \rightarrow 1} dt \Theta^{(3)}|_t, \end{aligned} \quad (26)$$

where the first line on the right hand side describes the case of no transition during the time interval  $dt$ , the second one the transition from state 2 to 1, and the third one the transition from state 3 to 1. Similar identities hold for  $\Theta^{(2)}$  and  $\Theta^{(3)}$ . Provided the system is stationary, i.e., the probabilities do not depend on time, one can omit the time dependent subscript and set  $\Theta^{(1)}|_{t+dt} = \Theta^{(1)}|_t = \Theta^{(1)}$ . Subtraction of  $\Theta^{(1)}$  on both sides and division by  $dt$  then give

$$0 = -\Gamma_{1 \rightarrow 2} \Theta^{(1)} - \Gamma_{1 \rightarrow 3} \Theta^{(1)} + \Gamma_{2 \rightarrow 1} \Theta^{(2)} + \Gamma_{3 \rightarrow 1} \Theta^{(3)}. \quad (27)$$

This is, of course, nothing else than a master equation of a stationary process. Its derivation has been given in order to prepare for the calculation in Sec. IV. The factors in front of  $\Theta^{(1)}$  (with the minus sign) represent the rates of all transitions which *must not* occur to maintain the considered state 1, while the factors in front of  $\Theta^{(2)}$  and  $\Theta^{(3)}$  (with the plus sign) are the rates of the transitions which *have to* occur in order to switch into state 1.

Prepared in this way, we return to our considered single-

file system. Although it has a vast number of configurations of the form  $(\sigma_1, \sigma_2, \dots, \sigma_N)$ , there are only a few transitions with nonzero probability starting from each of these configurations. Each such transition corresponds to a hop of a particle from an occupied site to a vacant neighboring site, from an occupied marginal site into the gas phase, or from the gas phase to a vacant marginal site, respectively. We give the complete set of equations at once in the form of Eq. (27) and explain it term by term afterwards. For each configuration  $(\sigma_1, \sigma_2, \dots, \sigma_N)$  one has an equation of the following form:

$$\begin{aligned} 0 = & -(\alpha(1 - \sigma_1) + \varepsilon \sigma_1(1 - \Omega \sigma_2)) \Theta^{\dots} \\ & - \Gamma \sum_{j=1}^{N-1} ((1 - \Omega \sigma_{j-1}) \sigma_j (1 - \sigma_{j+1}) + (1 - \sigma_j) \sigma_{j+1} (1 - \Omega \sigma_{j+2})) \Theta^{\dots} \\ & - ((1 - \Omega \sigma_{N-1}) \sigma_N \varepsilon + (1 - \sigma_N) \alpha) \Theta^{\dots} \\ & + (\alpha \sigma_1 + \varepsilon (1 - \sigma_1) (1 - \Omega \sigma_2)) \Theta^{(1 - \sigma_1) \dots} \\ & + \Gamma \sum_{j=1}^{N-1} ((1 - \Omega \sigma_{j-1}) (1 - \sigma_j) \sigma_{j+1} + \sigma_j (1 - \sigma_{j+1}) (1 - \Omega \sigma_{j+2})) \Theta^{\dots \sigma_{j+1} \sigma_j \dots} \\ & + ((1 - \Omega \sigma_{N-1}) (1 - \sigma_N) \varepsilon + \sigma_N \alpha) \Theta^{\dots (1 - \sigma_N)} \\ & \forall \sigma_1, \dots, \sigma_N = 0, 1. \end{aligned} \quad (28)$$

So far, this set of equations has no unique solution because the equations add up to zero. The missing equation is provided by the obvious identity

$$\sum_{\sigma_1=0}^1 \dots \sum_{\sigma_N=0}^1 \Theta^{\sigma_1 \dots \sigma_N} = 1. \quad (29)$$

Here and in all the following equations we abbreviate the upper index “ $\sigma_1 \sigma_2 \dots \sigma_N$ ” by dots “ $\dots$ ” indicating explicit deviations from the normal order only, i.e.,  $\Theta^{\dots}$  means  $\Theta^{\sigma_1 \sigma_2 \dots \sigma_N}$ ,  $\Theta^{(1 - \sigma_1) \dots}$  means  $\Theta^{(1 - \sigma_1) \sigma_2 \dots \sigma_N}$ , etc.

The two terms in each line of Eq. (28) always correspond to the transitions due to hops between the same pair of neighbor sites (or between a marginal site and the gas phase, respectively) but in opposite directions. First consider lines 1–3 (minus sign) which correspond to transitions that would make the system *leave* the considered configuration  $(\sigma_1, \dots, \sigma_N)$ . Line 1 considers the transitions due to hops between the gas phase and site 1.  $\alpha(1 - \sigma_1)$  is the transition rate due to adsorption events; it is proportional to the adsorption rate  $\alpha$  of the isolated particle but zero in the case of  $\sigma_1 = 1$  (i.e., site 1 occupied).  $\varepsilon \sigma_1(1 - \Omega \sigma_2)$  represents the transition rate due to desorption events; again it contains the respective rate  $\varepsilon$  and the factor  $\sigma_1$  being zero if site 1 is vacant. The remaining factor  $(1 - \Omega \sigma_2)$  has regard to the attractive interaction between neighboring molecules: it is equal to 1 if the neighboring site is vacant ( $\sigma_2 = 0$ ) but equal

to  $\omega$  if the hopping particle feels the attractive force of a particle at site 2 ( $\sigma_2 = 1$ ); here we have made use of the abbreviation

$$\Omega = 1 - \omega. \quad (30)$$

The  $(N - 1)$ -fold line 2 describes all transitions due to hops between the site pairs  $j, j + 1$ . Their rates are proportional to  $\Gamma$ . The left term stands for a hop from site  $j$  to site  $j + 1$ ; its rate is nonzero for  $\sigma_j = 1, \sigma_{j+1} = 0$  only; the factor  $(1 - \Omega \sigma_{j-1})$  represents the interaction influence as discussed before. Analogously, the right term considers the backward hop. Finally, line 3 is the mirror analog to line 1 describing the adsorption and desorption processes at the right margin.

Now we turn to the transitions which *lead* to configuration  $(\sigma_1, \dots, \sigma_N)$  (lines 4–6, plus sign). The structure of these lines is very similar to that of lines 1–3 because the transitions correspond to the same particle hops. They differ, though, in two points.

The probability factor  $\Theta^{\dots}$  is replaced by the probability of the starting configuration where the respective transition goes out. Note that the starting configurations for hops that only differ in their directions have, nevertheless, an equal mathematical form since, in both cases, the two sites involved in the hop simply exchange their  $\sigma$  value. Of course, there is no starting configuration for which the two transition rates (i.e., the two terms on the line) are nonzero simultaneously.

In each term, factors of the form  $(1 - \sigma_i)$  are replaced by  $\sigma_i$  and vice versa. This is because the values of  $\sigma_i$  now correspond to the configuration *after* the transition, while in lines 1–3 they had corresponded to the configuration *before* the transition. The interaction factors  $(1 - \Omega \sigma_i)$  remain unaffected since they do not change during the transition.

We have to supplement that in lines 2 and 5 the convention

$$\sigma_0 = 0, \quad \sigma_{N+1} = 0 \quad (31)$$

has been assumed in order to prevent further splitting of these lines into special cases.

### B. The residence time distributions

In analogy to Eq. (24) we define joint probability densities replacing the densities  $\varphi_i^*(\tau)$  of Eq. (10)

$$\varphi_i^{\sigma_1 \cdots \sigma_{i-1} * \sigma_{i+1} \cdots \sigma_N}(\tau) d\tau = P(\sum_1 = \sigma_1, \dots, \sum_{i-1} = \sigma_{i-1}, \sum_i = 1, \sum_{i+1} = \sigma_{i+1}, \dots, \sum_N = \sigma_N, \tau \leq \tau_i < \tau + d\tau). \quad (32)$$

In addition to the upper index of the  $\Theta^{\sigma_1 \cdots \sigma_N}$ , the  $\varphi_i^{\sigma_1 \cdots \sigma_{i-1} * \sigma_{i+1} \cdots \sigma_N}(\tau)$  wear a lower index  $i$  corresponding to that of the  $\varphi_i^*(\tau)$ . It gives the number of the ‘‘tagged’’ site: This site is meant to be occupied, and the particle occupying it has spent a time between  $\tau$  and  $\tau + d\tau$  within the system [cf. Eq. (32)]. That is why the upper index now contains the asterisk holding the place of the missing  $\sigma_i$  which would always be equal to 1. The upper and lower index together now distinguish the  $N \times 2^{N-1}$  quantities defined in Eq. (32). (In contrast, the upper index of the  $\Theta^{\sigma_1 \cdots \sigma_N}$  can distinguish between  $2^N$  quantities.) Again, the densities  $\varphi_i^*(\tau)$  can be computed from the joint densities by

$$\begin{aligned} \varphi_i^*(\tau) &= \Theta_i \varphi_i(\tau) = \sum_{\sigma_1=0}^1 \cdots \sum_{\sigma_{i-1}=0}^1 \sum_{\sigma_{i+1}=0}^1 \cdots \\ &\quad \times \sum_{\sigma_N=0}^1 \varphi_i^{\sigma_1 \cdots \sigma_{i-1} * \sigma_{i+1} \cdots \sigma_N}(\tau). \end{aligned} \quad (33)$$

To establish a set of equations for the joint densities  $\varphi_i^{\sigma_1 \cdots \sigma_{i-1} * \sigma_{i+1} \cdots \sigma_N}(\tau)$ , we first consider the fictional three-state system again. If we write Eq. (26) for  $\tau$ -dependent quantities  $\varphi^{(1)}(\tau), \varphi^{(2)}(\tau), \varphi^{(3)}(\tau)$ , we have to pay special attention to the argument. Since  $\tau$  means the time a particle

has already spent within the system, it increases by  $dt$  as the time proceeds by  $dt$ . Consequently, we have to write

$$\begin{aligned} \varphi^{(1)}(\tau + dt)|_{t+dt} &= (1 - \Gamma_{1 \rightarrow 2} dt - \Gamma_{1 \rightarrow 3} dt) \varphi^{(1)}(\tau)|_t \\ &\quad + \Gamma_{2 \rightarrow 1} dt \varphi^{(2)}(\tau)|_t + \Gamma_{3 \rightarrow 1} dt \varphi^{(3)}(\tau)|_t. \end{aligned} \quad (34)$$

If we now proceed as before [omitting the time subscript, subtraction of  $\varphi^{(1)}(\tau)$ , and division by  $dt$ ]  $\varphi^{(1)}(\tau)$  does not cancel against  $\varphi^{(1)}(\tau + dt)$  and we obtain, in the limit  $dt \rightarrow 0$ , the first derivative with respect to  $\tau$ . The analog of Eq. (27), therefore, reads

$$\begin{aligned} \frac{d}{d\tau} \varphi^{(1)}(\tau) &= -\Gamma_{1 \rightarrow 2} \varphi^{(1)}(\tau) - \Gamma_{1 \rightarrow 3} \varphi^{(1)}(\tau) + \Gamma_{2 \rightarrow 1} \varphi^{(2)}(\tau) \\ &\quad + \Gamma_{3 \rightarrow 1} \varphi^{(3)}(\tau). \end{aligned} \quad (35)$$

Therefore, in order to get an equation for the joint probabilities  $\varphi_i^{\sigma_1 \cdots \sigma_{i-1} * \sigma_{i+1} \cdots \sigma_N}$  one has to replace the zero on the left hand sides in Eq. (28) by the first derivative. Further changes are due to the different forms of the indices: Each time the respective hop involves the tagged site indicated by the lower index  $i$ , some lines of the equation take a special form. Again, we write the set of equations in full and explain it afterwards.

$$\begin{aligned} \frac{d}{d\tau} \varphi_i^{\cdots} &= -(\alpha(1 - \sigma_1) + \varepsilon \sigma_1(1 - \Omega \sigma_2)) \varphi_i^{\cdots} \\ &\quad - \Gamma \sum_{j=1}^{N-1} ((1 - \Omega \sigma_{j-1}) \sigma_j (1 - \sigma_{j+1}) + (1 - \sigma_j) \sigma_{j+1} (1 - \Omega \sigma_{j+2})) \varphi_i^{\cdots} \\ &\quad - ((1 - \Omega \sigma_{N-1}) \sigma_N \varepsilon + (1 - \sigma_N) \alpha) \varphi_i^{\cdots} \\ &\quad + (\alpha \sigma_1 + \varepsilon(1 - \sigma_1)(1 - \Omega \sigma_2)) \begin{cases} \delta(\tau) \Theta^{0 \sigma_2 \cdots \sigma_N}, & i=1 \\ \varphi_i^{(1 - \sigma_1) \cdots}, & \text{else} \end{cases} \end{aligned}$$

$$\begin{aligned}
& + \Gamma \sum_{j=1}^{N-1} ((1-\Omega\sigma_{j-1})(1-\sigma_j)\sigma_{j+1} + \sigma_j(1-\sigma_{j+1})(1-\Omega\sigma_{j+2})) \left\{ \begin{array}{l} \varphi_{i+1}^{\dots\sigma_{i-1}0*\sigma_{i+2}\dots}, \quad i=j \\ \varphi_{i-1}^{\dots\sigma_{i-2}0*\sigma_{i+1}\dots}, \quad i=j+1 \\ \varphi_i^{\dots\sigma_{j+1}\sigma_j\dots}, \quad \text{else} \end{array} \right. \\
& + ((1-\Omega\sigma_{N-1})(1-\sigma_N)\varepsilon + \sigma_N\alpha) \left\{ \begin{array}{l} \delta(\tau)\Theta^{\sigma_1\dots\sigma_{N-1}0}, \quad i=N \\ \varphi_i^{\dots(1-\sigma_N)}, \quad \text{else} \end{array} \right. \\
& \forall \sigma_1, \dots, \sigma_{i-1}, \sigma_{i+1}, \dots, \sigma_N = 0, 1; \quad i = 1, \dots, N,
\end{aligned} \tag{36}$$

with the initial condition

$$\varphi_i^{\dots}(0) = 0. \tag{37}$$

The relatively compact form of the set is possible only with the additional convention

$$\sigma_i = 1. \tag{38}$$

Moreover, we omitted the argument which is always  $(\tau)$ . Note that the abbreviated upper index of the  $\varphi_i^{\dots}$  contains the asterisk instead of  $\sigma_i$ :  $\varphi_i^{\dots}$  means  $\varphi_i^{\sigma_1\dots\sigma_{i-1}*\sigma_{i+1}\dots\sigma_N}$ , etc.

The rate coefficients in Eq. (36) are completely equal to that of Eq. (28) because the underlying transitions are all the same. The change in the index connected with the respective transition, however, has now a different mathematical form in certain cases which, therefore, had to be separated. Consider first line 5. The ‘‘else’’ branch corresponds to the ‘‘normal’’ case, as in Eq. (28). If  $i=j$  the transition is due to a hop either from the tagged site  $i$  to site  $i+1$  or from site  $i+1$  to the tagged site  $i$ . The former case cannot lead to the considered configuration (where  $\sigma_i=1$ ) and need, therefore, not be considered [the convention Eq. (38) automatically cancels the corresponding rate coefficient]. In the latter case, the particle which occupies the tagged site after the transition, came from site  $i+1$ ; that is why the variable with the lower index  $i+1$  has to be used here instead of that with  $i$ . Its upper index reflects the situation before the hop: site  $i$  was vacant (indicated by the 0 in the place of  $\sigma_i$ ), site  $i+1$  was occupied (here indicated by the \* because of the formation law of the indices), the other sites were unaffected. Finally, the case  $i=j+1$  means hops between site  $i-1$  and the tagged site  $i$  and has to be treated in an analogous way.

Now consider line 4 which deals with transitions due to hops between site 1 and the gas phase. If site 1 is not the tagged one we again have the ‘‘normal’’ case. The special case is  $i=1$ . Again, the convention Eq. (38) provides a zero transition rate in the case of desorption. In the case of ad-

sorption, however, the particle occupying the tagged site 1 after the transition came from the gas phase, i.e., it did not spend any time within the channel. Therefore, the density of its residence time is given by  $\delta(\tau)$ . In order to obtain the joint probability density needed here it has to be multiplied by the probability of the configuration before the transition which is characterized by  $\sigma_1=0$ .

A similar argument applies to line 6. Lines 1–3 are similar to that of Eq. (28): Since no transition occurs, no special cases have to be considered.

### C. The reactant concentration profile

As indicated by Eq. (20) the profile of the reactant concentration can be obtained from the densities of the residence times by Laplace transformation. Thus we define

$$\eta_i^{\sigma_1\dots\sigma_{i-1}*\sigma_{i+1}\dots\sigma_N} = \int_0^\infty e^{-k\tau} \varphi_i^{\sigma_1\dots\sigma_{i-1}*\sigma_{i+1}\dots\sigma_N}(\tau) d\tau. \tag{39}$$

Laplace transformation of Eq. (33) then gives

$$\eta_i^* = \sum_{\sigma_1=0}^1 \dots \sum_{\sigma_{i-1}=0}^1 \sum_{\sigma_{i+1}=0}^1 \dots \sum_{\sigma_N=0}^1 \eta_i^{\sigma_1\dots\sigma_{i-1}*\sigma_{i+1}\dots\sigma_N}. \tag{40}$$

A linear set of equations determining the quantities  $\eta_i^{\sigma_1\dots\sigma_{i-1}*\sigma_{i+1}\dots\sigma_N}$  is most easily obtained by Laplace transformation of the set Eq. (36). Taking into consideration that

$$\int_0^\infty e^{-k\tau} \left( \frac{d}{d\tau} \varphi_i^{\dots}(\tau) \right) d\tau = k \eta_i^{\dots} \tag{41}$$

[cf. Eq. (37)] and

$$\int_0^\infty e^{-k\tau} \delta(\tau) d\tau = 1, \tag{42}$$

one gets

$$\begin{aligned}
0 &= -k \eta_i^{\dots} \\
& - (\alpha(1-\sigma_1) + \varepsilon\sigma_1(1-\Omega\sigma_2)) \eta_i^{\dots} \\
& - \Gamma \sum_{j=1}^{N-1} ((1-\Omega\sigma_{j-1})\sigma_j(1-\sigma_{j+1}) + (1-\sigma_j)\sigma_{j+1}(1-\Omega\sigma_{j+2})) \eta_i^{\dots} \\
& - ((1-\Omega\sigma_{N-1})\sigma_N\varepsilon + (1-\sigma_N)\alpha) \eta_i^{\dots}
\end{aligned}$$

$$\begin{aligned}
 & + (\alpha\sigma_1 + \varepsilon(1 - \sigma_1)(1 - \Omega\sigma_2)) \begin{cases} \Theta^{0\sigma_2 \cdots \sigma_N}, & i = 1 \\ \eta_i^{(1-\sigma_1) \cdots}, & \text{else} \end{cases} \\
 & + \Gamma \sum_{j=1}^{N-1} ((1 - \Omega\sigma_{j-1})(1 - \sigma_j)\sigma_{j+1} + \sigma_j(1 - \sigma_{j+1})(1 - \Omega\sigma_{j+2})) \begin{cases} \eta_{i+1}^{\cdots\sigma_{i-1}0^*\sigma_{i+2}\cdots}, & i = j \\ \eta_{i-1}^{\cdots\sigma_{i-2}0^*\sigma_{i+1}\cdots}, & i = j + 1 \\ \eta_i^{\cdots\sigma_{j+1}\sigma_j\cdots}, & \text{else} \end{cases} \\
 & + ((1 - \Omega\sigma_{N-1})(1 - \sigma_N)\varepsilon + \sigma_N\alpha) \begin{cases} \Theta^{\sigma_1 \cdots \sigma_{N-1}0}, & i = N \\ \eta_i^{\cdots(1-\sigma_N)}, & \text{else} \end{cases} \\
 & \forall \sigma_1, \dots, \sigma_{i-1}, \sigma_{i+1}, \dots, \sigma_N = 0, 1; \quad i = 1, \dots, N.
 \end{aligned} \tag{43}$$

The inhomogeneity of this set consists in the terms with  $\Theta^{0\sigma_2 \cdots \sigma_N}$  and  $\Theta^{\sigma_1 \cdots \sigma_{N-1}0}$  in lines 4 and 6, respectively, which are known from the solution of Eq. (28).

**D. The moments**

If the Laplace transformation in the preceding section is replaced by the ‘‘transformation’’ given in Eq. (12) one gets the moments  $^{(m)}\mu_i$  and their mean  $^{(m)}\mu$ . As before, we define

$$^{(m)}\mu_i^{\sigma_1 \cdots \sigma_{i-1}^* \sigma_{i+1} \cdots \sigma_N} = \int_0^\infty \tau^m \varphi_i^{\sigma_1 \cdots \sigma_{i-1}^* \sigma_{i+1} \cdots \sigma_N}(\tau) d\tau, \tag{44}$$

yielding the weighted moments

$$^{(m)}\mu_i^* = \Theta_i \ ^{(m)}\mu_i = \sum_{\sigma_1=0}^1 \cdots \sum_{\sigma_{i-1}=0}^1 \sum_{\sigma_{i+1}=0}^1 \cdots \sum_{\sigma_N=0}^1 \ ^{(m)}\mu_i^{\sigma_1 \cdots \sigma_{i-1}^* \sigma_{i+1} \cdots \sigma_N} \tag{45}$$

and, finally,  $^{(m)}\mu$ , due to Eq. (13). Applying the transformation Eq. (12) to the set Eq. (36), we now observe that

$$\int_0^\infty \tau^m \left( \frac{d}{d\tau} \varphi_i^{\cdots}(\tau) \right) d\tau = [\tau^m \varphi_i^{\cdots}(\tau)]_{\tau=0}^\infty - \int_0^\infty m \tau^{m-1} \varphi_i^{\cdots}(\tau) d\tau = -m \ ^{(m-1)}\mu_i^{\cdots} \tag{46}$$

and

$$\int_0^\infty \tau^m \delta(\tau) d\tau = 0, \tag{47}$$

and we get

$$\begin{aligned}
-m \binom{m-1}{i} \mu_i^{\dots} &= -(\alpha(1-\sigma_1) + \varepsilon\sigma_1(1-\Omega\sigma_2)) \binom{m}{i} \mu_i^{\dots} \\
&\quad - \Gamma \sum_{j=1}^{N-1} ((1-\Omega\sigma_{j-1})\sigma_j(1-\sigma_{j+1}) + (1-\sigma_j)\sigma_{j+1}(1-\Omega\sigma_{j+2})) \binom{m}{i} \mu_i^{\dots} \\
&\quad - ((1-\Omega\sigma_{N-1})\sigma_N\varepsilon + (1-\sigma_N)\alpha) \binom{m}{i} \mu_i^{\dots} \\
&\quad + (\alpha\sigma_1 + \varepsilon(1-\sigma_1)(1-\Omega\sigma_2)) \begin{cases} 0, & i=1 \\ \binom{m}{i} \mu_i^{(1-\sigma_1)\dots}, & \text{else} \end{cases} \\
&\quad + \Gamma \sum_{j=1}^{N-1} ((1-\Omega\sigma_{j-1})(1-\sigma_j)\sigma_{j+1} + \sigma_j(1-\sigma_{j+1})(1-\Omega\sigma_{j+2})) \begin{cases} \binom{m}{i} \mu_{i+1}^{\dots\sigma_{i-1}0^*\sigma_{i+2}\dots}, & i=j \\ \binom{m}{i} \mu_{i-1}^{\dots\sigma_{i-2}^0\sigma_{i+1}\dots}, & i=j+1 \\ \binom{m}{i} \mu_i^{\dots\sigma_{j+1}\sigma_j\dots}, & \text{else} \end{cases} \\
&\quad + ((1-\Omega\sigma_{N-1})(1-\sigma_N)\varepsilon + \sigma_N\alpha) \begin{cases} 0, & i=N \\ \binom{m}{i} \mu_i^{\dots(1-\sigma_N)}, & \text{else} \end{cases} \\
\forall \sigma_1, \dots, \sigma_{i-1}, \sigma_{i+1}, \dots, \sigma_N = 0, 1; & \quad i = 1, \dots, N. \tag{48}
\end{aligned}$$

Now the inhomogeneity is due to the terms  $-m \binom{m-1}{i} \mu_i^{\dots}$  on the left side, which are known if the moments are calculated successively. On calculating the first moments one has to use

$$\binom{0}{i} \mu_i^{\dots} = \int_0^\infty \varphi_i^{\dots}(\tau) d\tau = \Theta^{\sigma_1 \dots \sigma_{i-1} 1 \sigma_{i+1} \dots \sigma_N}, \tag{49}$$

which are solutions of Eq. (28). The factors “0” in the cases  $i=1$  and  $i=N$ , simply mean that the respective line vanishes.

#### IV. RESULTS AND DISCUSSION

The sets of equations (28), (48), and (43) deduced in the preceding section were implemented into a computer program which solved them using the Gauss algorithm. In this way, the dependence of the profiles,  $\Theta_i$ ,  $\binom{1}{i} \mu_i$ ,  $\eta_i^*$ , and their means or totals,  $\Theta$ ,  $\binom{1}{i} \mu$ ,  $H^*$ , on the system parameters could be studied. Scattered within the whole parameter range, the validity of the results was checked by comparison with the results of Monte Carlo simulations (using an algorithm similar to that described in [12]) confirming full conformity.

For a number of reasons it is convenient to introduce *dimensionless parameters*, as had been done in [12]. The parameter

$$v = \frac{\varepsilon}{\alpha} = \frac{\hat{\varepsilon}}{\hat{\alpha}} e^{-E_M/RT} \tag{50}$$

gives the ratio of the rates of adsorption and desorption of the isolated particle and is, therefore, tightly connected with the sorption equilibrium. To get rid of the parameter  $\Gamma$  we choose the average time between successive hops of an iso-

lated particle,  $\tau = 1/2\Gamma$ , as a unit of the time scale and define the *relative particle exchange rate*

$$a = \frac{\alpha}{2\Gamma} = \frac{\hat{\alpha}}{2\hat{\Gamma}} e^{-(E_B)/RT} \tag{51}$$

and, for the conversion, the *relative reaction rate*

$$\kappa = \frac{k}{2\Gamma} = \frac{\hat{k}}{2\hat{\Gamma}} e^{-(E_R - E_B)/RT}. \tag{52}$$

The remaining parameters  $N$  and  $\omega$  are already dimensionless by definition. The new set of parameters now is  $v$ ,  $\omega$ ,  $a$ ,  $\kappa$ , and  $N$ .

Unfortunately, the parameter range accessible by the algorithm is subject to considerable numerical limitations. By far the most serious one is the limitation of the file length  $N$  by memory size problems. Even using a special version of the Gauss algorithm taking advantage of the rather sparse coefficient matrix, the memory space needed is of the order  $2^N \times N 2^{N-1}$  multiplied by the number of bytes per coefficient. The computer equipment at our disposal, therefore, allowed a maximum of  $N=11$ . But even if these memory limitations could be overcome, the computation time sets its limit approximately at the same place, since it increases with increasing  $N$  due to a power law with an exponent of at least 4. That is why all algorithms swapping parts of the matrix to the disc are of no use here. Iterative procedures like Gauss-Seidel cannot help either because the matrix does not fulfill their convergence criteria [17]. Although invoking the symmetry of the system would reduce the number of equations per set by a factor of the order of 2 this corresponds merely to a gain in  $N$  by 1; instead, the symmetry would be lost as a means of checking for numerical instability. Recent tests,

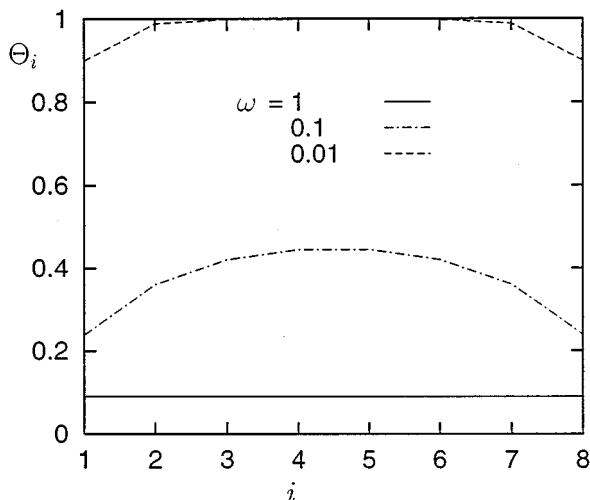


FIG. 4. Concentration profile  $\Theta_i$  over the site number  $i$  for  $v=10$  and different strengths of the attractive particle-particle interaction.

however, suggest that the conjugate gradient method might be a promising way to increase the maximal value of the system size  $N$ . In all calculations presented here, we chose  $N=8$  as a compromise between computation time needed and information gained.

The second limitation affects the range of the parameter  $k$  in the calculation of  $\eta_i^*$ . Since the coefficient in front of  $\eta_i^{**}$  (i.e., the diagonal element of the matrix) contains a sum roughly of the form  $N+k/\Gamma$ , the numerical accuracy (number of digits) of the computer sets a lower limit to the parameter  $\kappa=2k/\Gamma$ . Using double accuracy, we reached  $\kappa \approx 10^{-14}$  without signs of numerical problems.

It is worth noting, however, that the range of parameters that can be evaluated by Monte Carlo simulations is limited as well. Although the file length can easily be chosen up to almost any value without memory trouble, the computation time necessary to reach sorption and reaction equilibrium is extraordinary. Tracer exchange studies for  $N=50$ , e.g., are a matter of weeks of uninterrupted computation. The range of  $\kappa$  is confined for the same reason to  $\kappa > 10^{-5}$  approximately. Thus, the use of the exact solution indeed provides new information. The authors are optimistic that, pending further computer development, the restrictions mentioned should be overcome in the future.

#### A. The concentration profile

In the case  $\omega=1$  (no attractive interaction of neighboring particles) the concentration profile is uniform:  $\Theta_i = 1/(1+v)\forall i$  [12]. With increasing strength of the attractive interaction (decreasing  $\omega$ ) the particles concentrate in the middle of the channel. Figure 4 shows some typical examples.

In Fig. 5 we present the dependence of the mean concentration  $\Theta$  on the parameters. The individual graphs show the dependence on the parameter  $v$  for different strengths of the attractive interaction (different values of the parameter  $\omega$ ). The stronger the attractive interaction the narrower is the region of  $v$  where the concentration changes from the almost

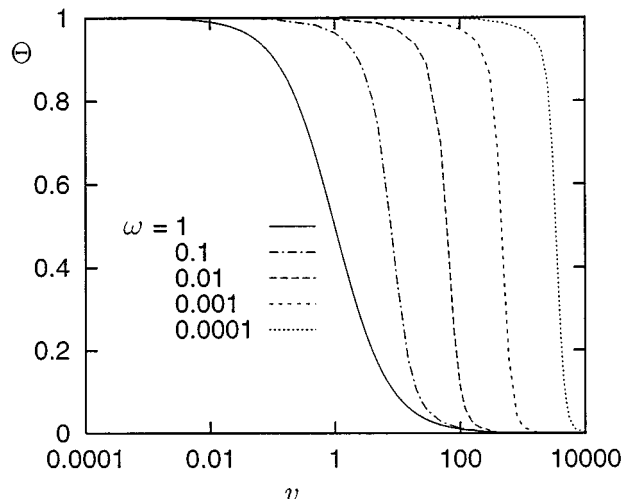


FIG. 5. Mean concentration  $\Theta$  over  $v$  for different strengths of the attractive particle-particle interaction.

complete occupation ( $\Theta \approx 1$ ) to the almost empty channel ( $\Theta \approx 0$ ). Outside this region, the mean concentration  $\Theta$  still varies with  $v$  (the linear plot deceives the eye): For large  $v$  we have an asymptotic behavior  $\Theta \propto 1/v$ , while for small  $v$  a similar relation holds for the “vacancy concentration”  $(1-\Theta) \propto v$ . The parameter  $a$  does not influence the concentration, as can be shown by the detailed-balance arguments.

#### B. The tracer exchange

Figure 6 shows the average intracrystalline residence time profile  ${}^{(1)}\mu_i$  for the same case as considered in Fig. 4. Note that this profile does *not* give the average time the particles have spent at the individual sites, but the average *total* time they have spent in the channel when reaching a certain site. As expected, this average time is largest in the center of the channel.

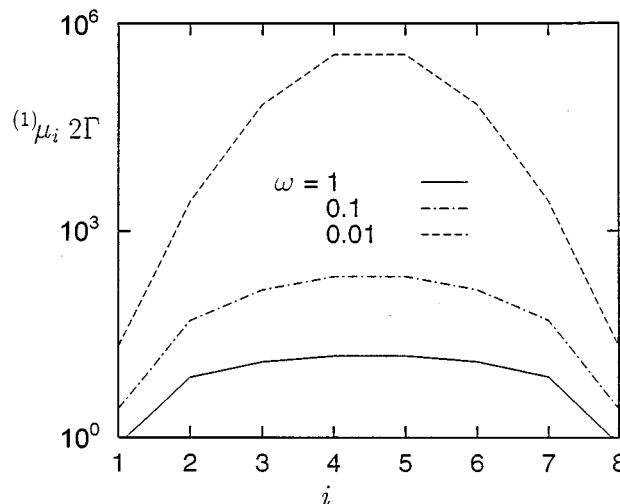


FIG. 6. Average intracrystalline residence time profile  ${}^{(1)}\mu_i$  (in units of  $\tau=1/2\Gamma$ ) over site number  $i$  for  $v=10$ ,  $a=0.5$ , and different strengths of the attractive particle-particle interaction.

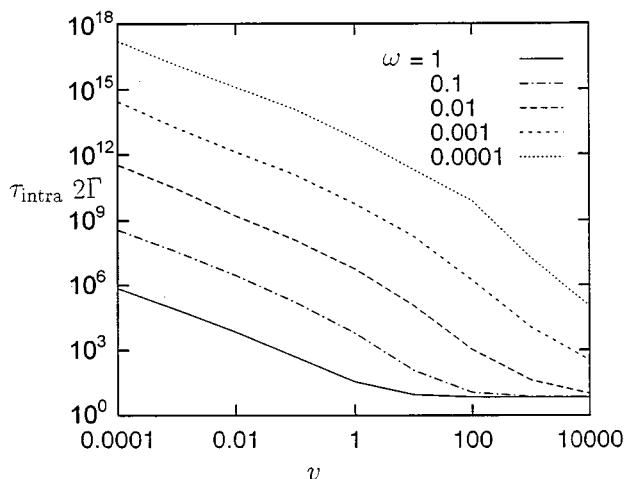


FIG. 7. Mean intracrystalline residence time  ${}^{(1)}\mu = \tau_{\text{intra}}$  (in units of  $\tau = 1/2\Gamma$ ) over  $v$  for  $a = 0.5$  and different strengths of the attractive particle-particle interaction.

The weighted mean of the first moments or the intracrystalline residence time  ${}^{(1)}\mu = \tau_{\text{intra}}$  is given in Fig. 7, parameter ranges and symbols chosen equal to Fig. 5. For each strength of the attractive interaction, one can distinguish three regions within the range of the parameter  $v$ : In the case of very small  $v$ , where the channel is almost completely occupied (cf. Fig. 5), one finds, most probably, not more than one ‘‘isolated vacancy’’ in the channel which determines the dynamics alone; the curves for the different values of the parameter  $\omega$  are parallel and obey a power law in  $v$ . In the opposite case, for large values of  $v$  where the channel is almost empty, one reaches the case of the isolated particle, i.e., the system loses its single-file nature and behaves according to normal diffusion. Therefore, the system response does not depend on the parameters  $v$  and  $\omega$  anymore, because the isolated particle is unaffected by changes in the concentration or the particle-particle interaction. The third region, the position of which depends on  $\omega$ , provides the transition between these two extreme cases and reveals the actual characteristics of single-file diffusion. One observes that the slope of the curves in this region increases with increasing strength of the attractive interaction, i.e., the attractive interaction enhances the sensitivity of the system response to changes in the parameter  $v$  (as was already seen in the dependence of the concentration  $\Theta$  on  $v$ ).

Figure 8 shows the influence of the margin on the mean residence time. For very small values of the parameter  $a$  the marginal barrier dominates the dynamics of the system. This influence, however, is driven back with increasing strength of the attractive interaction.

### C. The catalytic reaction

In Fig. 9, the reactant concentration profile at several relative reaction rates is given and compared with the total concentration profile ( $\kappa = 0$ ). In the middle of the channel where particle exchange with the gas phase is slow, the reactant concentration drops. If the parameters are adjusted so that the residence times in the channel center are large enough, or simply if the channel is sufficiently long, the reactant con-

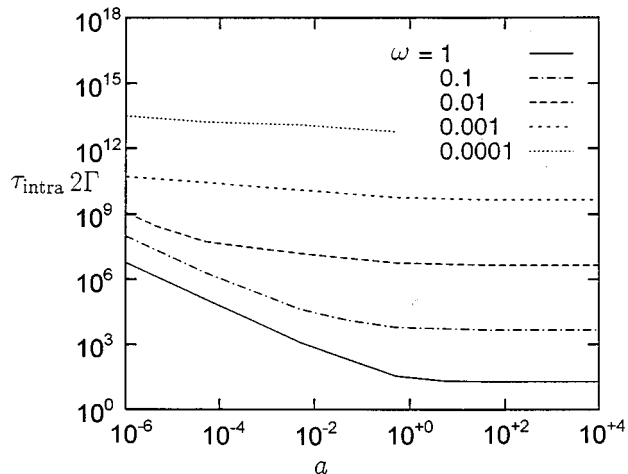


FIG. 8. Mean intracrystalline residence time  ${}^{(1)}\mu = \tau_{\text{intra}}$  (in units of  $\tau = 1/2\Gamma$ ) dependent on the relative rate of particle exchange at the margin (parameter  $a$ ) for  $v = 1$  and different strengths of the attractive particle-particle interaction.

centration in the middle of the channel reaches zero (cf. the case  $\kappa = 1$  in Fig. 9). In this case, the mean number of reactant molecules  $H^*$ , does not increase any more if the file length  $N$  increases; i.e., the values of  $H^*$  calculated for such cases are equally valid for arbitrarily longer channels [12].

In comparison with  $\tau_{\text{intra}}$ ,  $H^*$  depends on a further parameter, the relative reaction rate  $\kappa$ . To show the dependence on all the parameters one would need a considerable number of diagrams. This is why a more compact representation is desirable. Moreover, we are particularly interested in the *temperature dependence* of the conversion under single-file conditions. For zeolitic single-file systems, the parameters, which most strongly vary with temperature, are  $\kappa$  and  $v$ , while the other parameters,  $a$ ,  $\omega$ , and  $N$ , are not, or only slightly, temperature dependent. It would, therefore, be most

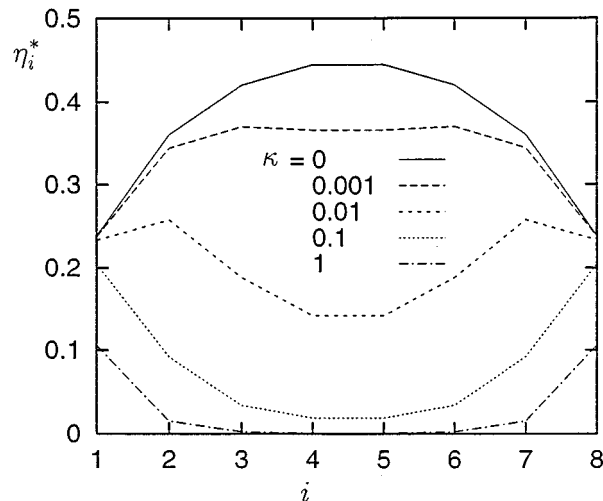


FIG. 9. Reactant concentration profile  $\eta_i^*$  for  $v = 10$ ,  $\omega = 0.1$ ,  $a = 0.5$ , and different values of the relative reaction rate  $\kappa$ . The curve for  $\kappa = 0$  (no conversion) coincides with the total concentration profile.

instructive to *simultaneously* show the influences of  $\kappa$  and  $\nu$  and their interplay. The isoline representation of  $H^*$ , already introduced in [12], meets all these requirements. In the plane of the parameters  $\kappa$  and  $\nu$ , the isolines connect all points with equal values of  $H^*$ . The *spacing* between adjacent isolines tells us how strong  $H^*$  varies with the parameters: Narrow spacings mean a strong dependence and vice versa. The *direction* of the isolines with respect to the axes reveals the relative influence of the two parameters: The parameter whose axis direction is nearer to the direction perpendicular to the isolines predominates in the considered parameter region. The temperature dependence can be read from the isoline representation in the following way [12]:

For fixed values of  $\hat{\varepsilon}$ ,  $\hat{\alpha}$ ,  $\hat{\Gamma}$ ,  $E_M$ ,  $E_B$ , and  $E_R$  [cf. Eqs. (50) and (52)], both  $(\ln \nu)$  and  $(\ln \kappa)$  are proportional to  $1/RT$ . Since we choose log axes in the  $(\kappa, \nu)$  plane, one simply moves on a straight line when varying the temperature. Every given temperature interval corresponds to a certain section of this straight line. The more isolines are crossed by such a fixed section, the stronger  $H^*$  depends on temperature (i.e., the higher is the absolute value of the “activation energy” of  $H^*$ ). If, with increasing temperature, the isolines are crossed in ascending order, the “activation energy” of  $H^*$  is positive, or vice versa. Once the straight line is fixed (i.e., the temperature dependence of the parameters  $\kappa$  and  $\nu$  is fixed) the activation energy of  $H^*$ , within a given temperature region, thus can be read directly from the direction of its isolines (or, more precisely, from the angle between the directions of the straight line and the isolines) and the mutual spacing between adjacent isolines. In the following we give the isoline representation for several choices of the relative exchange rate  $a$  and the interaction parameter  $\omega$ .

Figure 10 shows the isolines of  $H^*$  for a system of fixed length  $N=8$  with rapid particle exchange at the margin ( $a=50$ ) and without attractive interaction ( $\omega=1$ ). This representation is very similar to that already given in [12] (there the limit  $a \rightarrow \infty$  was considered, and the file length  $N$  was chosen large enough to ensure zero reactant concentration in the channel center, so that the representation was valid for any sufficiently long channel). The topology of Fig. 10 can be understood in the following way. Consider first a line parallel to the  $\kappa$  axis for a small value of  $\nu$  where the file is almost completely occupied ( $\Theta \approx 1$ ). In the lower region of the figure, where the reaction is fast, i.e., at large values of  $\kappa$ , the molecules are converted soon after they enter the channel. This leads to a very small number  $H^*$  of reactant molecules within the file. If  $\kappa$  is decreased, i.e., the conversion becomes slower,  $H^*$  increases, ultimately to reach  $\Theta N \approx N=8$ , when almost all molecules in the channel remain reactants until they leave. If  $\kappa$  is further decreased,  $H^*$  cannot increase any more, so that no more isolines follow above. Now fix the parameter  $\kappa$  at such a small value and increase the parameter  $\nu$ . Then,  $\Theta$  decreases from  $\approx 1$  to  $\approx 0$  according to Fig. 5. Consequently,  $H^*$  decreases from  $\approx N$  to  $\approx 0$ . In Fig. 10, this is expressed by the region of isolines parallel to the  $\kappa$  axis. (Of course, there are infinitely more isolines for  $H^* < 0.46$  which, however, are omitted. They would simply fill up the entire right part of the diagram, as well as the left lower corner.) Finally, consider a large value of  $\kappa$ , e.g.,  $\kappa = 10^{-2}$ , and vary the parameter  $\nu$

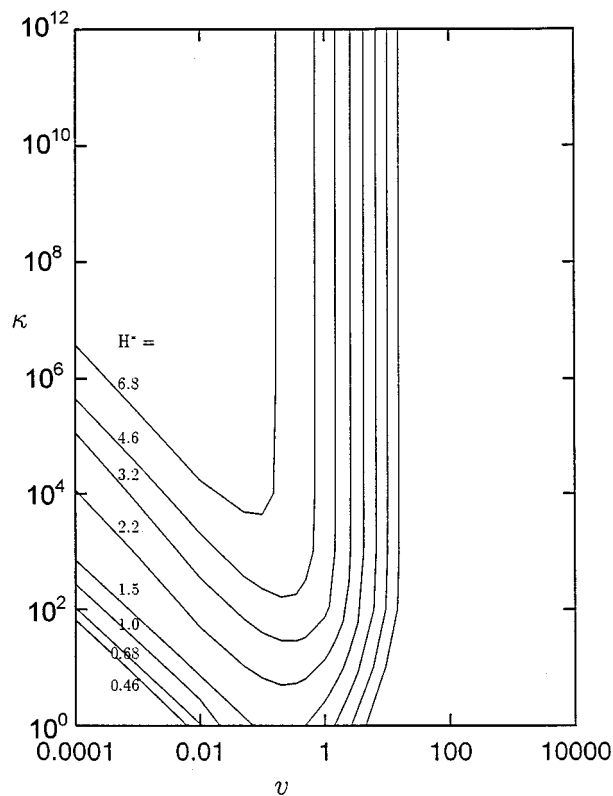


FIG. 10. Isolines of the mean number of reactant molecules per channel  $H^*$ , on the  $(\kappa, \nu)$ -parameter space for  $a=50$ ,  $\omega=1$ . (All isolines below  $H^*=0.46$  are omitted.)

again. In this case, there is a maximum of  $H^*$  approximately in the middle of the represented  $\nu$  range resulting from the competition of two contrary effects. If  $\nu$  is decreased from a high value the total number of particles in the file increases so that, as in the case of small  $\kappa$ ,  $H^*$  might increase. Simultaneously, however, the mutual hindrance of the particles increases so that their mobility drops and their residence times increase (cf. the increasing mean residence time at decreasing values of  $\nu$  in Fig. 7). If the time the particles stay in the channel is long, their chance to be converted is high, so that the number  $H^*$  of reactant particles eventually decreases.

Now we reduce the particle exchange at the margin. In Fig. 11 the case  $a=0.5$  is considered. The direction of the isolines is still the same as for the rapid exchange, but the narrower spacings show that the sensitivity to the parameters has increased. Moreover, for constant  $\kappa$  the maximum of  $H^*$  has translated to larger values of the parameter  $\nu$  (since the concentration does not depend on  $a$ , this means that the maximum is now attained at a lower concentration).

Finally, we investigate the influence of the attractive interaction. We choose  $\omega=10^{-4}$  which is the strongest interaction of those considered before, see Fig. 12. There is a further translation of the isoline pattern to larger values of  $\nu$ , this time connected with the translation already observed in the dependence of the concentration  $\Theta$  on  $\nu$  (see Fig. 5). For values of  $H^*$  larger than 2 (corresponding to the case in which more than only the two marginal sites contribute to the reaction), however, we observe a drastic change in the

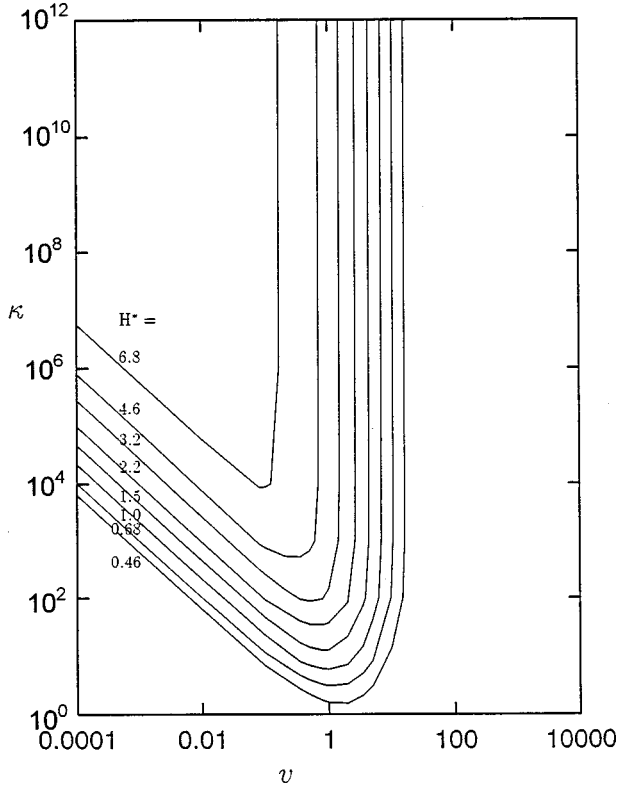


FIG. 11. Isolines of the mean number of reactant molecules per channel  $H^*$ , on the  $(\kappa, \nu)$ -parameter space for  $a=0.5$ ,  $\omega=1$ . (All isolines below  $H^*=0.46$  are omitted.)

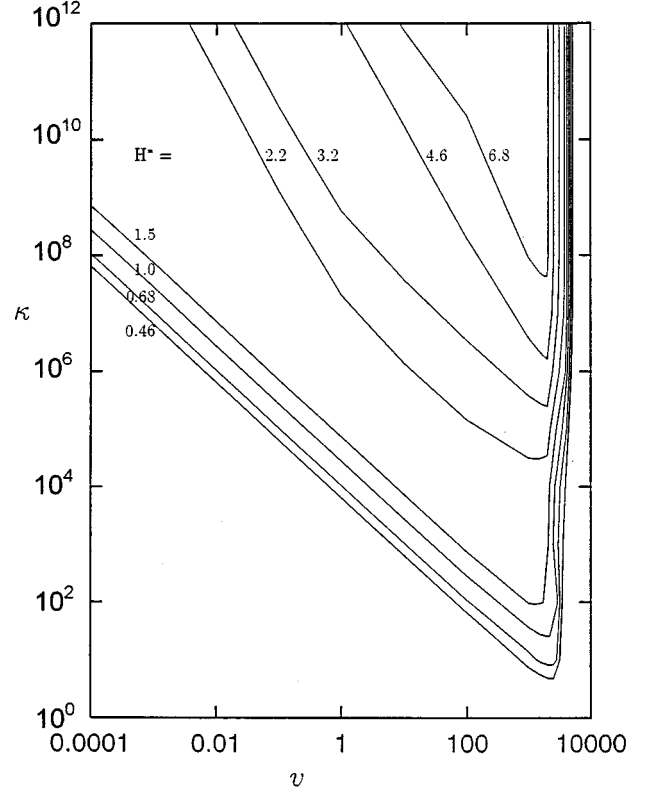


FIG. 12. Isolines of the mean number of reactant molecules per channel  $H^*$ , on the  $(\kappa, \nu)$ -parameter space for  $a=0.5$ ,  $\omega=10^{-4}$ . (All isolines below  $H^*=0.46$  are omitted.)

direction of the isolines; obviously the parameter  $\nu$  gains a stronger influence in this parameter region. As we already stated before, the attractive interaction increases the sensitivity to the parameter  $\nu$ . The steeper direction of the isolines expresses a change in the temperature dependence: The attractive particle-particle interaction *enhances the activation energy* of  $H^*$ .

#### D. Correlations

In Sec. III we stated as a premise that the stochastic variables  $\Sigma_i$  and  $\tau_i$  are dependent on each other, and that these correlations are responsible for the necessity of such gigantic sets of equations. In order to get an idea of their strength and range we inspect the correlation coefficients. To start with, take the occupation-occupation dependence,

$$\begin{aligned} \varrho(\Sigma_i, \Sigma_j) &= \frac{\langle (\Sigma_i - \langle \Sigma_i \rangle) (\Sigma_j - \langle \Sigma_j \rangle) \rangle}{\sqrt{\langle (\Sigma_i - \langle \Sigma_i \rangle)^2 \rangle \langle (\Sigma_j - \langle \Sigma_j \rangle)^2 \rangle}} \\ &= \frac{\sum_{(\sigma_1 \dots \sigma_N)} \Theta^{\sigma_1 \dots \sigma_N} (\sigma_i - \Theta_i) (\sigma_j - \Theta_j)}{\sqrt{(\Theta_i - \Theta_i^2) (\Theta_j - \Theta_j^2)}}, \end{aligned} \quad (53)$$

where the sum is extended over all configurations,  $\sum_{(\sigma_1 \dots \sigma_N)} = \sum_{\sigma_1=0}^1 \dots \sum_{\sigma_N=0}^1$ . Without the attractive

particle-particle interaction  $\omega=1$ , the occupations at different sites are independent from each other,  $\varrho(\Sigma_i, \Sigma_j) = \delta_{i,j}$ . With increasing interaction strength, the dependence increases, as is shown in Fig. 13 for  $\omega=0.0001$  and  $\nu=4000$  ( $\Theta=0.249$ ). This plot proves that the range of the correlations comprises the whole length of the channel, i.e., every

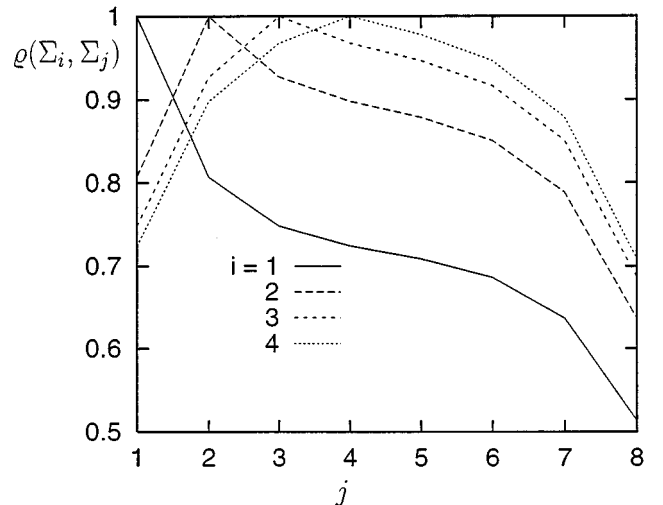


FIG. 13. Correlation coefficient  $\varrho(\Sigma_i, \Sigma_j)$  for  $\omega=0.0001$ ,  $\nu=4000$  as a profile.

site is dependent on every other one. The strength of these correlations, however, varies with the parameters. As a measure of the overall correlations we define

$$\varrho_{\Sigma\Sigma} = \sqrt{\sum_{i \neq j} [\varrho(\Sigma_i, \Sigma_j)]^2} \quad (54)$$

and give its dependence on the parameters  $\nu$  and  $\omega$  see Fig. 14 (the symbols are equal to Fig. 5). The maxima of the curves lie in the transition region between the almost completely occupied and the almost empty channel. This is indeed expected: In the almost empty file one has correlation-free normal diffusion, while the processes in the almost completely occupied file can be considered as ‘‘normal diffusion of a vacancy.’’ This indicates once more that the single-file character of the system is most pronounced in the region in between.

Likewise, we investigate the correlations between the residence times and the occupation via the correlation coefficient

$$\varrho(\tau_i, \Sigma_j) = \frac{\langle (\tau_i - \langle \tau_i \rangle)(\Sigma_j - \langle \Sigma_j \rangle) \rangle}{\sqrt{\langle (\tau_i - \langle \tau_i \rangle)^2 \rangle \langle (\Sigma_j - \langle \Sigma_j \rangle)^2 \rangle}} = \frac{\sum_{(\sigma_1 \dots \sigma_{i-1} \sigma_{i+1} \dots \sigma_N)} \int_{\tau=0}^{\infty} d\tau \varphi_i(\tau) - {}^{(1)}\mu_i(\sigma_j - \Theta_j)}{\sqrt{({}^{(2)}\mu_i - [{}^{(1)}\mu_i]^2)(\Theta_j - \Theta_j^2)}} \quad (55)$$

(here the sum extends only over all configurations with  $\sigma_i = 1$ ), whose profile is shown in Fig. 15. If a site is occupied the particle obstructs the way of the other particles so that the positive correlation is understandable. Figure 16 gives the total correlation

$$\varrho_{\tau\Sigma} = \sqrt{\sum_{i \neq j} [\varrho(\tau_i, \Sigma_j)]^2}. \quad (56)$$

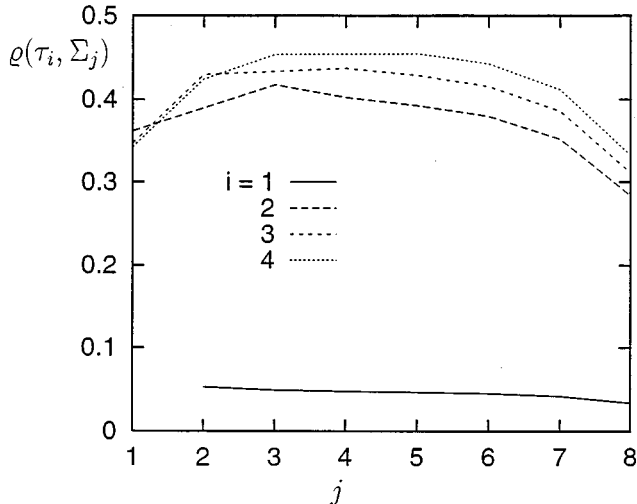


FIG. 15. Correlation coefficient  $\varrho(\tau_i, \Sigma_j)$  for  $\omega = 0.0001$ ,  $\nu = 4000$ ,  $a = 0.5$  as a profile.

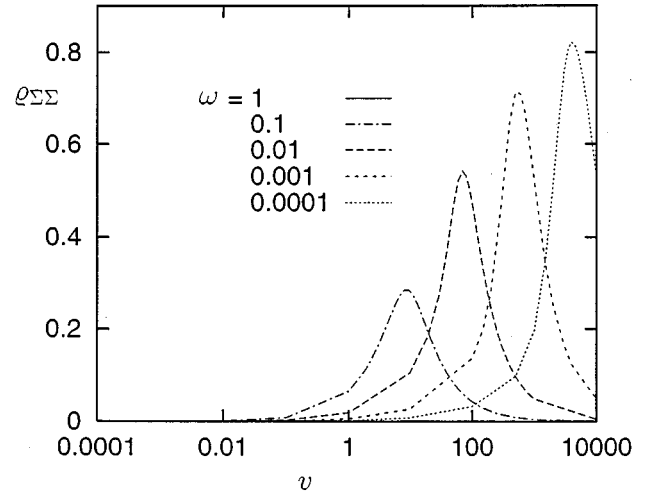


FIG. 14. Overall occupation-occupation correlation  $\varrho_{\Sigma\Sigma}$  dependent on the parameters  $\nu$  and  $\omega$ .

In contrast to  $\varrho_{\Sigma\Sigma}$ , the correlation  $\varrho_{\tau\Sigma}$  is perceptible over the whole range of  $\nu$  and, in particular, does *not* vanish for  $\omega = 1$ . These correlation coefficients confirm that the use of the joint probabilities of  $\Sigma_i$  and  $\tau_i$  is indeed indispensable.

### E. The residence time distributions

Finally, we give an example of the residence time distributions itself. The curves were obtained according to Eq.

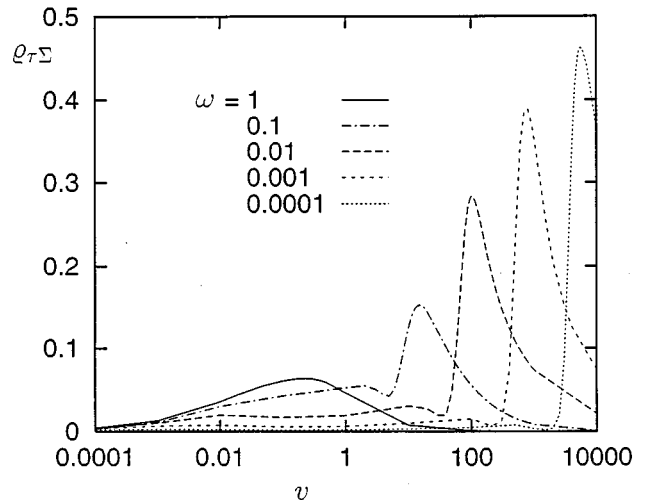


FIG. 16. Overall correlation between residence time and occupation,  $\varrho_{\tau\Sigma}$ , dependent on the parameters  $\nu$  and  $\omega$  ( $a = 0.5$ ).

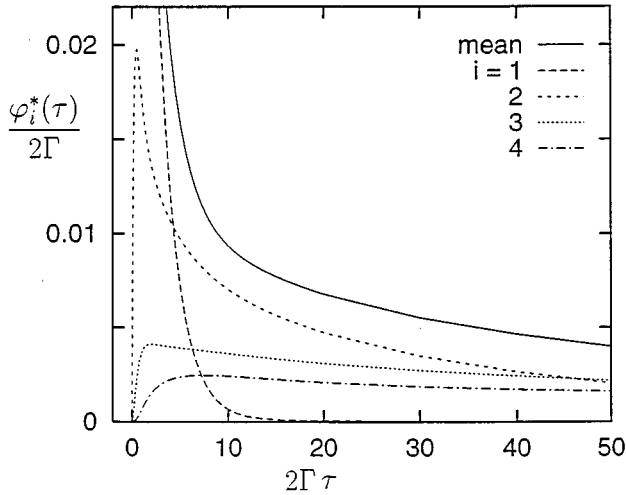


FIG. 17. Intracrystalline residence time distributions  $\varphi_i^*(\tau)$  at sites  $i=1, \dots, 4$  and their mean  $\varphi(\tau)$  for  $N=8$ ,  $v=10$ ,  $\omega=0.1$ , and  $a=0.5$ .

(36) by an adapted Runge-Kutta algorithm. In this case, the memory problems are less serious, while the necessary computation time is considerable.

Figure 17 shows the distributions for a special set of parameters for sites  $i=1, \dots, 4$  (the curves for the other half of the channel,  $i=5, \dots, 8$  are, of course, identical) together with the mean residence time distribution according to Eq. (11). In Fig. 18 the same curves are plotted for a larger time interval and on a log scale. The straight lines in this plot, for sufficiently long times, indicate that, in this region, all residence time distributions become single exponentials with a common exponent [the least eigenvalue of the set Eq. (36) of linear differential equations].

The figures show that the mean residence time distribution  $\varphi(\tau)$  is a monotonously decreasing function,

$$\frac{d}{d\tau}\varphi(\tau) < 0 \quad \forall \tau, \quad (57)$$

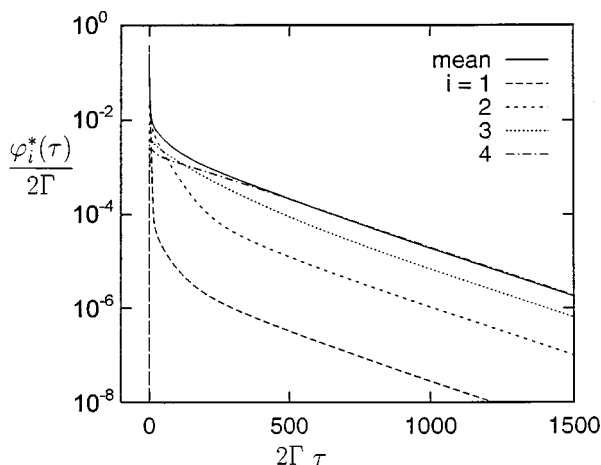


FIG. 18. Intracrystalline residence time distributions  $\varphi_i^*(\tau)$  and their mean  $\varphi(\tau)$  on a log scale. Parameters as in Fig. 17.

thus having its maximum at  $\tau=0$ . This is true for the mean residence time distribution of *any* diffusional channel, as can be understood in a line of argumentation reminiscent of the derivation of Eq. (36). Consider the channel at two arbitrary consecutive instants of time  $t$  and  $t+\Delta t$ , and consider an arbitrary residence time  $\tau$ . At time  $t$ , there will be  $P$  particles in the channel having a residence time between  $\tau$  and  $\tau+d\tau$ . At time  $t+\Delta t$ , some of these particles will have left the file while a certain part, say  $P'$  with  $P' < P$ , is still in the channel and has, of course, now a residence time between  $\tau+\Delta t$  and  $\tau+\Delta t+d\tau$ . On the other hand, *no further* particles than these can, at  $t+\Delta t$ , have such a residence time. Thus  $P'$  is the number of *all* particles having a residence time between  $\tau+\Delta t$  and  $\tau+\Delta t+d\tau$ . Since we assumed stationarity of the transport processes we need not pay any attention to the time and may, in accordance with Eq. (11), write  $\langle P \rangle = \Theta N \varphi(\tau) d\tau$  and  $\langle P' \rangle = \Theta N \varphi(\tau+\Delta t) d\tau$ . From  $P' < P$  we have  $\langle P' \rangle < \langle P \rangle$ , whence Eq. (57) is confirmed.

## V. CONCLUSION

The stationary single-file system may be characterized by the concentration profile  $\Theta_i$  and the residence time distributions  $\varphi_i(\tau)$ . From these probabilities, important quantities such as the mean intracrystalline residence time  $\tau_{\text{intra}} = {}^{(1)}\mu$  and the effectiveness factor  $\eta$  can be found. We derived sets of linear equations determining all these quantities. As a consequence of the strong correlations in the single-file system, the necessary number of equations per set is extremely high. For sufficiently short channels, however, the sets of equations can be solved numerically. In this way, the principal dependence of these quantities on the system parameters could be studied.

Currently, the presented derivation is applied to a much wider class of single-file systems as well, including channels with *unequal sites*, consideration of the residence time at a certain *subset of sites* or even individual sites, systems where the mutual passage of molecules within the channel is *not excluded completely*, *reversible reactions*, *mixtures* of the particle species outside the channel, conversion between particles with *unequal transport properties*, and *long-range particle-particle interactions*.

Some remarks concerning *detailed balance* may be added. It can be shown that the configurations satisfy a detailed-balance relation, i.e., the ratio of the probabilities of two arbitrary configurations is equal to the ratio of the transition rates between them. Using this relation the probabilities  $\Theta^{\sigma_1 \dots \sigma_N}$  can be found in a much easier way than via Eq. (28). We did not succeed, however, in finding an equivalent relation for the quantities  $\eta^{\sigma_1 \dots \sigma_N}$ . The reason is that these quantities correspond to the *steady state* of the conversion which might be interpreted as a driven diffusion. Driven diffusive systems, however, are known not to fulfill detailed balance. Finding similar relations is an important aim of future work because this could considerably simplify the numerical procedure and, in this way, facilitate the investigation of larger or more sophisticated systems.

## ACKNOWLEDGMENT

The authors thank Professor Klaus W. Kehr for continuous encouragement and for his suggestion to consider the attractive particle-particle interaction. Stimulating discus-

sions with Dr. Lothar Partzsch are gratefully acknowledged. The authors are obliged to the Studienstiftung des Deutschen Volkes and to the Deutsche Forschungsgemeinschaft (SFB 294) for financial support of this work.

- 
- [1] P. A. Fedders, *Phys. Rev. B* **17**, 40 (1978).
- [2] H. van Beijeren, K. W. Kehr, and R. Kutner, *Phys. Rev. B* **28**, 5711 (1983).
- [3] H. Spohn, *Large Scale Dynamics of Interacting Particles* (Springer, Berlin, 1991).
- [4] J. Kärger, M. Petzold, H. Pfeifer, S. Ernst, and J. Weitkamp, *J. Catal.* **136**, 283 (1992).
- [5] J. Kärger, *Phys. Rev. A* **45**, 4173 (1992); *Phys. Rev. E* **47**, 1427 (1993).
- [6] P. M. Richards, *Phys. Rev. B* **16**, 1393 (1977).
- [7] A. L. Hodgkin and R. D. Keynes, *J. Phys.* **128**, 91 (1955).
- [8] W. H. Meier, D. H. Olson, and Ch. Baerlocher, *Atlas of Zeolite Structure Types* (Elsevier, London, 1996).
- [9] See, e.g., *Studies in Surface Science and Catalysis*, edited by J. Weitkamp, H. Karge, H. Pfeifer, and W. Hölderich (Elsevier, Amsterdam, 1994), Vol. 84C.
- [10] V. Gupta, S. S. Nivarthi, A. V. McCormick, and H. T. Davis, *Chem. Phys. Lett.* **247**, 596 (1995); V. Kukla, J. Kornatowski, D. Demuth, I. Girnus, H. Pfeifer, L. Rees, S. Schunk, K. Unger, and J. Kärger, *Science* **272**, 702 (1996); K. Hahn, J. Kärger, and V. Kukla, *Phys. Rev. Lett.* **76**, 2762 (1996).
- [11] Z. Karpiński, S. N. Ghandi, and W. M. H. Sachtler, *J. Catal.* **141**, 337 (1993); G. D. Lei, B. T. Carvill, and W. M. H. Sachtler, *Appl. Catal.* **142**, 347 (1996).
- [12] C. Rödenbeck, J. Kärger, and K. Hahn, *J. Catal.* **157**, 656 (1995).
- [13] Models of this type have widely been used to describe the diffusional behavior of molecules in zeolites successfully see, e.g., R. M. Barrer, *J. Chem. Soc. Faraday Trans.* **86**, 1123 (1990).
- [14] P. C. Carman and R. A. W. Haul, *Proc. R. Soc. London, Ser. A* **222**, 109 (1954).
- [15] J. Kärger and D. M. Ruthven, *Diffusion in Zeolites and Other Microporous Solids* (Wiley-Interscience, New York, 1992).
- [16] W. O. Haag, R. M. Lago, and P. B. Weisz, *Discuss. Faraday Soc.* **72**, 317 (1982).
- [17] E. Isaacson and H. Keller, *Analyse Numerischer Verfahren* (Edition Leipzig, Leipzig, 1972).